Journal of Crystal Growth 480 (2017) 62–66

Contents lists available at ScienceDirect

Journal of Crystal Growth

journal homepage: www.elsevier.com/locate/crys

Growth and characterization of $Na_2Mo_2O_7$ crystal scintillators for rare event searches

Indra Raj Pandey [a], H.J. Kim [a,*], Y.D. Kim [b]

[a] Department of Physics, Kyungpook National University, Daegu 41566, Republic of Korea
[b] Center for Underground Physics, Institute for Basic Science (IBS), Daejeon 34047, Republic of Korea

ARTICLE INFO

Article history:
Received 10 May 2017
Received in revised form 21 September 2017
Accepted 28 September 2017
Available online 30 September 2017
Communicated by T.F. Kuech

Keywords:
B1. Disodium dimolybdate crystal
A2. Czochralski technique
A1. X-ray diffraction
B3. Crystal scintillators

ABSTRACT

Disodium dimolybdate ($Na_2Mo_2O_7$) crystals were grown using the Czochralski technique. The thermal characteristics of the compound were analyzed using thermogravimetric analysis (TGA) and differential scanning calorimetry (DSC) measurements. The crystal structure of the grown sample was confirmed using X-ray diffraction (XRD). Luminescence properties were measured at room and low temperatures, using a light emitting diode (LED) source. Very weak luminescence was observed at room temperature; however, the luminescence intensity was enhanced at low temperatures. The crystal's transmittance spectrum was measured for estimating its optical quality and energy band gap. The grown crystal exhibited a luminescence light yield of 55% compared with $CaMoO_4$ crystals at 10 K, when excited by a 280-nm-wavelength LED source, but does not have the drawbacks of radioactive Ca isotopes. These results suggest that at cryogenic temperatures, $Na_2Mo_2O_7$ crystal scintillators are promising for the detection of dark matter and neutrinoless double beta decay of ^{100}Mo.

1. Introduction

Deep underground rare event search experiments, such as detection of neutrinoless double beta ($0\nu2\beta$) decay [1] and weakly interacting massive particles (WIMPs) as dark matter candidates [2], provide opportunities for discovering new physics to complement high-energy physics.

The experimental search for neutrinoless double beta decay is the only feasible way for testing the Majorana nature of neutrinos [3]. Many experimental groups throughout the world have been actively searching for $0\nu2\beta$ in ^{76}Ge, ^{96}Zr, ^{124}Sn, ^{110}Pb, ^{130}Te, ^{136}Xe, ^{82}Se, ^{150}Nd, ^{100}Mo, ^{48}Ca, and ^{116}Cd candidate isotopes [4]. Among these isotopes, ^{100}Mo is one of the most promising candidates, owing to its high transition energy ($Q_{\beta\beta} = 3034.40 \pm 0.17$ keV) [5], comparative ease of enrichment [6] and higher natural abundance ($\delta = 9.744\ (65)\ \%$) [7]. Several Mo-based crystal scintillators have been developed, including $PbMoO_4$ [8], $SrMoO_4$ [9], $MgMoO_4$ [10], $CdMoO_4$ [11], $ZnMoO_4$ [12,13], Li_2MoO_4 [14], and $CaMoO_4$ [15]. The Advanced Mo-based Rare process Experiment (AMoRE) collaboration has been searching for neutrinoless double beta decay of the ^{100}Mo isotope using $^{40}Ca^{100}MoO_4$ crystals [16] in a deep underground laboratory, to minimize the possible background effect owing to cosmic radiation. Compared with other molybdate crystals, $CaMoO_4$ has a highest scintillator efficiency at cryogenic [17] and room [15,18] temperatures. The main drawback of the $CaMoO_4$ crystal is the presence of ^{48}Ca, which is a $2\upsilon2\beta$ active isotope [14]. Moreover, it is very challenging to purify Ca-based compounds with acceptable radioactivity levels, owing to the limitations of Ca chemistry [17]. Thus, the AMoRE experimental group has been searching for new molybdate-based compounds. Regarding the dark matter search, KIMS [19], COSINE [20] and DAMA/LIBRA [21] groups have been using NaI:Tl crystal scintillators as target materials. On the other hand, CRESST [22] was the first to use $CaWO_4$ in a cryogenic dark matter search experiment [17,23], owing to its high light yield at cryogenic temperatures.

In this paper, we report the growth and luminescence properties of a novel $Na_2Mo_2O_7$ single crystal, grown by using the Czochralski technique. To the best of our knowledge, this is the first study to report the growth of $Na_2Mo_2O_7$ crystal. The advantages of this crystal are the absence of radioactive elements and the fact that purification techniques have been well-developed for both Na [19,21] and Mo [24]. In the future, because $Na_2Mo_2O_7$ crystal-based scintillators have a high luminescence light yield at cryogenic temperatures, they will be likely used for both $0\nu2\beta$ and WIMP searches in the same detector setup. The use of these crystals for validating the DAMA/LIBRA [21] annual modulation claims is also envisioned.

* Corresponding author.
E-mail address: hongjoo@knu.ac.kr (H.J. Kim).

https://doi.org/10.1016/j.jcrysgro.2017.09.031
0022-0248/

2. Materials and methods

2.1. Crystal growth

The $Na_2Mo_2O_7$ crystals were grown using the conventional Czochralski technique. The polycrystalline compound of $Na_2Mo_2O_7$ has been synthesized using the standard solid state reaction technique. High-purity powders of Na_2CO_3 (99.997%, Alfa Aesar) and MoO_3 (99.95%, Alfa Aesar) were used as starting materials for synthesis. The powders were taken in the following stoichiometric ratio:

$$Na_2CO_3 + 2MoO_3 \rightarrow Na_2Mo_2O_7 + CO_2 \uparrow \quad (1)$$

The powders were weighted inside a glove box to avoid contamination. The weighted powders and ceramic balls were put together in to a clean plastic bottle and mixed thoroughly for 24 h using the ball milling technique with the speed of 135 rpm (revolutions per minute). The resulting mixed powder was moved to an aluminum crucible, covered, and sintered at 530 °C for 15 h. For good sintering, the sintered powder was grinded in an agate mortar, following the sintering process with the same temporal profile was repeated at 540 °C. The well-sintered powder was transferred into a platinum crucible with the dimensions of 30 mm (Ø) × 30 mm (L), and into the Czochralski chamber for crystal growth. Ceramic fire-processed bricks and alumina were used as a thermal shield inside a radio frequency (RF) coil that acted to reduce the temperature gradient of the pulled crystal. The temperature in the crucible was monitored using a thermocouple that was coupled to the crucible at the bottom via hole that was drilled in the fire-processed brick and aluminum shield. For the first run, a 2.5-mm-diameter platinum rod was used as a seed material for growing the $Na_2Mo_2O_7$ crystal. An inert atmosphere was created inside the chamber by evacuating (2×10^{-2} Torr) and then refilling it with argon gas (11 Torr), repeating the procedure twice. The powder was heated upto the melting point, at the rate of 2 °C/min. The entire powder charged melted at 603 °C, and this temperature was maintained for 5 h to ensure a homogeneous melt. A platinum rod was dipped a few millimeters into the melt and was left in the melt for 1 h before starting the pulling process. Nucleation of the compound started at the tip of the rod owing to the temperature gradient of the rod and melt. The seed was uniformly rotated so that no stagnant regions were produced in the melt, precluding the formation of inclusions in the crystal. During the growth of the crystal, the pulling and rotation speeds were maintained at 1.5 mm/h and 10 rpm, respectively. At the termination of the crystal growth process, the crucible was cooled down to room temperature at the rate of 12 °C/h. Although the crystal has some cracks, using the above-described method we were able to grow ~20-mm-diameter and ~35-mm-long crystals successfully. Fig. 1 shows the $Na_2Mo_2O_7$ crystals grown using this method. From the grown crystal, we cut a $\sim 10 \times 10 \times 8$ mm^3 sample for further characterization using a homemade wire saw and a diamond-coated stainless steel wire. The remaining part of the crystal was used as a seed for re-growing additional crystals.

For additional growth, a single crystalline seed $\sim 2 \times 2 \times 15$ mm^3 was used from a previously grown $Na_2Mo_2O_7$ crystal. About ~1 mm length of the seed was inserted into the melt, the temperature in which was ~20 °C higher than the melting temperature of the compound, and nucleation started after a certain period of time. After that, pulling was started at the rate of ~1.5 mm/h, with the temperature decreasing at the rate of ~0.5 °C/h. These parameters were set for making a long neck, for obtaining crack-free crystals. Using a seed from this crystal, we were also able to grow large-size crystals (i.e., $\sim$Ø40 × 100 mm^3). However, larger crystals exhibited some cracks.

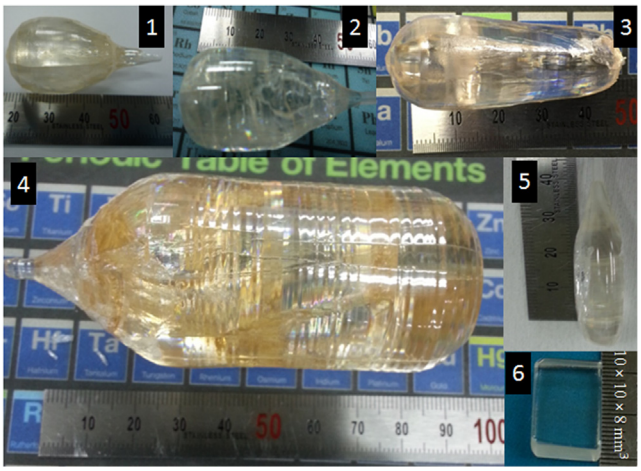

Fig. 1. Photographs of the grown crystals and samples with different dimensions: (1) Ø20 × 35 mm^3, (2) Ø20 × 40 mm^3, (3) Ø20 × 50 mm^3, (4) Ø40 × 100 mm^3, (5) Ø18 × 40 mm^3 and (6) 10 × 10 × 8 mm^3.

We measured the hygroscopicity of $Na_2Mo_2O_7$ and Li_2MoO_4 crystals and compared the results. For the hygroscopicity measurements, several pieces of both crystals were taken out from the mineral oil and dried inside the glove box. For both crystals, the crystal pieces were grind into fine powders and equal amounts of each powder were used. The two samples were kept in an open environment at room temperature, with the relative humidity of ~30%. Changes in the masses of the two powder samples were recorded every 24 h, for 10 days. The increase in mass of $Na_2Mo_2O_7$ and Li_2MoO_4 crystals are 0.0003 g and 0.0008 g respectively. The obtained result illustrates that $Na_2Mo_2O_7$ crystals are less hygroscopic than Li_2MoO_4 crystals.

2.2. Instrumental analysis

Powder XRD analysis of the grown crystals was conducted using a Philips XPERT-MED X-ray diffractometer using Cu Kα_1 radiation (λ = 0.154 nm); the scanning step size was 0.02° and time interval per step was 3.5 s. The generator voltage and the tube current used for scanning were 40 kV and 30 mA, respectively. TGA/DSC of $Na_2Mo_2O_7$ was conducted using a thermal analysis (TA) instrument SDT-Q600 that performs thermogravimetric analysis with differential scanning calorimetry (TGA-DSC). The sample was heated from 200 to 1000 °C in an aluminum crucible, with gaseous nitrogen flowing at a rate of 100 ml/min and with a heating rate of 4 °C/min. Transmittance spectra were recorded using a V-650 spectrophotometer (Jasco). Temperature-dependent luminescence was studied by exciting the sample using a LED source (wavelength, 280 nm). The crystal was cooled down in a refrigerator using compressed helium gas, and the temperature was controlled using a Lakeshore temperature controller Model 331. The emission spectrum was measured using a spectrometer (QE65000, Ocean Optics), for wavelengths ranging from 200 to 1000 nm. The spectral sensitivity of the spectrometer was corrected with a linearity correction of >99.8%. Thermally stimulated luminescence (TSL) was studied using an in-house experimental setup consisting of a bi-alkali photomultiplier tube (PMT Photonis XP2260), an X-ray generator (Cu anode), a cryogenics setup with a closed-cycle helium refrigerator, and a counter. First, the sample was irradiated with X-rays for 1 h at 10 K, and then heated from 10 K to 300 K, at a heating rate of 0.1 K/s; the obtained signals yielded typical TSL glow curves.

3. Results and discussion

3.1. Powder X-ray diffraction

Fig. 2 shows the XRD pattern obtained for the grown crystal. The diffraction peaks were compared with the ICSD 98-002-4312 standard reference data and matched the reference data quite well, as shown in Fig. 2. Analysis of the diffraction peaks revealed that the crystallized sample had an orthorhombic structure with the space group Cmca. The values of the measured lattice parameters were: a = 7.1640 Å, b = 11.8370 Å, c = 14.9130 Å, and $\alpha = \beta = \gamma = 90°$.

3.2. TGA/DSC analysis

The results of the TGA/DSC analysis are shown in Fig. 3. The mass loss in the TGA curve was mainly in the 200–647 °C (−2.27%) and 647–1000 °C (−18.29%) temperature regions. The mass loss in the first region was owing to the loss of some volatile substance absorbed by the powder during its preparation and phase transition, and the mass loss in the second region was attributed to the compound's decomposition. Fig. 3 also reveals two endothermic peaks at 522 °C and 603 °C, which corresponded to the solid state phase transition and melting of the compound, respectively. At high temperatures, orthorhombic crystals change to monoclinic ones [25]. Thus, care needs to be taken to obtain crack-free crystals. The sharp endothermic peak in the DSC curve reveals the good degree of crystallinity of the grown compound.

3.3. Ultraviolet–visible to near-infrared spectral analysis

The light collection efficiency of a scintillator increases with increasing transmittance [17]. The transmittance spectrum of the

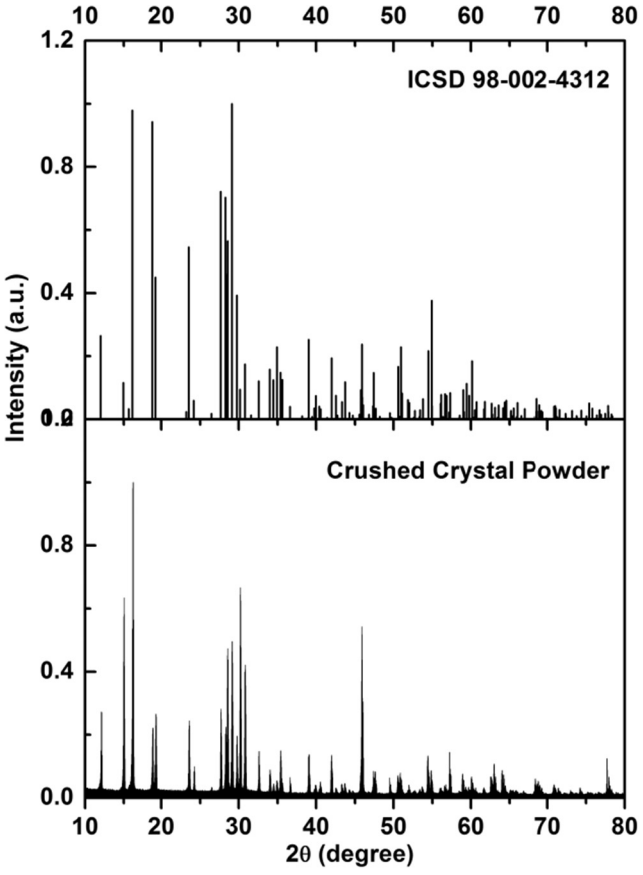

Fig. 2. Powder XRD patterns of the $Na_2Mo_2O_7$ crystal.

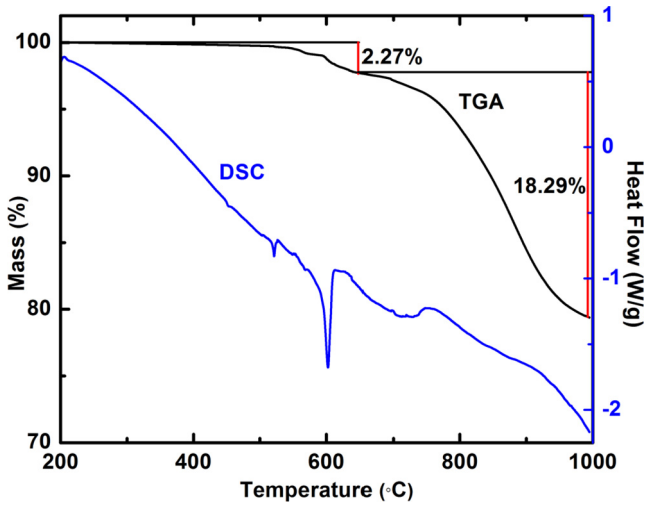

Fig. 3. TGA/DSC curves for the $Na_2Mo_2O_7$ single crystal. The mass loss shown on the TGA curve in the 200–647 °C range is 2.27%, whereas that in the 647–1000 °C range is 18.29%.

$Na_2Mo_2O_7$ crystal is shown in Fig. 4. The crystal is transparent throughout a wide spectral range, from 368 nm to 900 nm. The transmittance varies from ~75% to ~67%, from the infrared to visible region. The short wavelength cutoff at 368 nm results from the fundamental absorption properties of the $Na_2Mo_2O_7$ crystal. Using the Tauc plot [26], the optical band gap energy (E_g) for the indirect transition was found to be 3.05 eV, as shown in the inset of Fig. 4.

3.4. Luminescence properties

Temperature dependence luminescence intensity of the $Na_2Mo_2O_7$ crystal was studied using a LED source, for temperatures ranging from 300 K to 10 K. As shown in Fig. 5, at room temperature the spectrum of the sample exhibits emission in the 425–775 nm range, peaking at 661 nm. On the other hand, at 10 K, emission is observed in the 400–987 nm range, peaking at 663 nm. Very weak luminescence was observed at room temperature. The luminescence intensity significantly increased at temperatures below 250 K and the maximum intensity was achieved at 10 K. The emission intensity at 10 K was ~180 times higher than that at room temperature.

Fig. 6 shows the total intensities for $CaMoO_4$, $Na_2Mo_2O_7$, and Li_2MoO_4 crystals, for different temperatures, including the systematic error of 7% that results from the position and/or angle dependence of the crystals. The reference ($CaMoO_4$) crystal has the highest light yield among all the $CaMoO_4$ crystals, as reported in the literature [27] as CMO-4 from the Institute for Materials (Lviv, Ukraine). For calculating the error bar, the luminescence spectra of the $CaMoO_4$ and $Na_2Mo_2O_7$ crystals were measured seven times, for temperatures ranging from 300 K to 10 K, in temperature steps of 25 K. For each temperature region, seven data points were obtained for each of the crystals, and root mean square (RMS) values were estimated. For each point, the error bar was in the 5–9% range. The average error was 7%, obtained by taking the average error of the entire temperature region's error percentage. Temperature dependence of the luminescence light yield of $CaMoO_4$ using a UV excitation source was similar to the previously reported one [28]. However, the response of scintillation materials to the UV radiation can be significantly differ from their responses to the gamma, beta, or nuclear recoil radiation [28] that are expected in double beta decay and dark matter search experiments. The luminescence light yield of $Na_2Mo_2O_7$ is very low between 250 K and

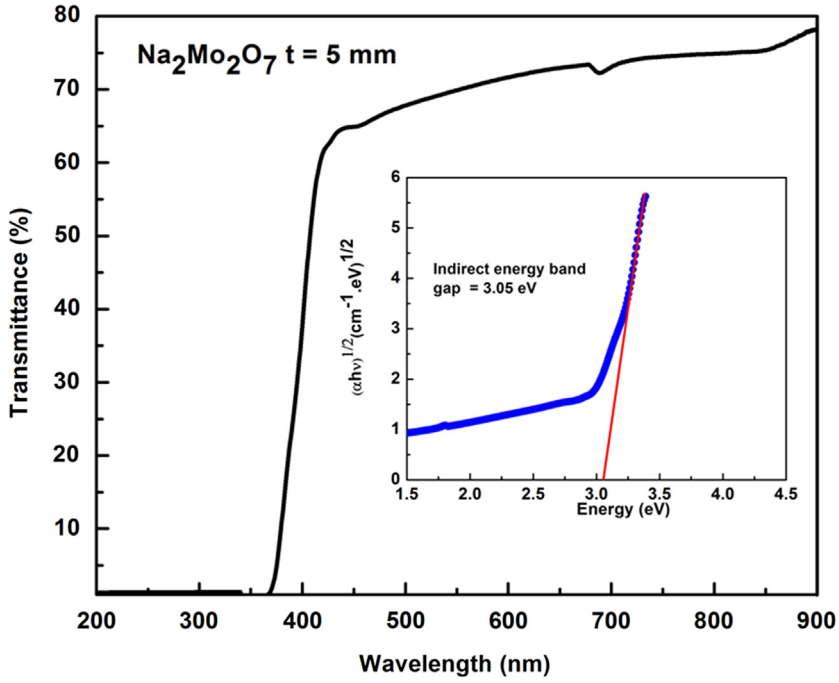

Fig. 4. Transmittance spectrum of the $Na_2Mo_2O_7$ crystal (thickness: t = 5 mm). The inset shows hυ vs. $(\alpha h\upsilon)^{1/2}$, for indirect energy band gap calculations.

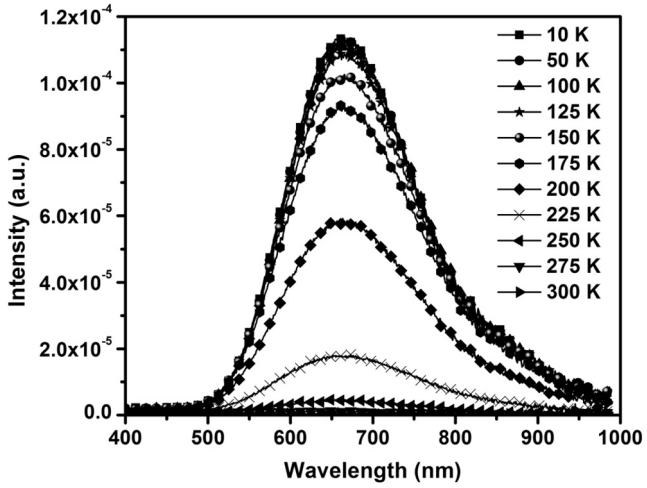

Fig. 5. Emission spectra of the $Na_2Mo_2O_7$ crystal, for temperatures ranging from 300 K to 10 K.

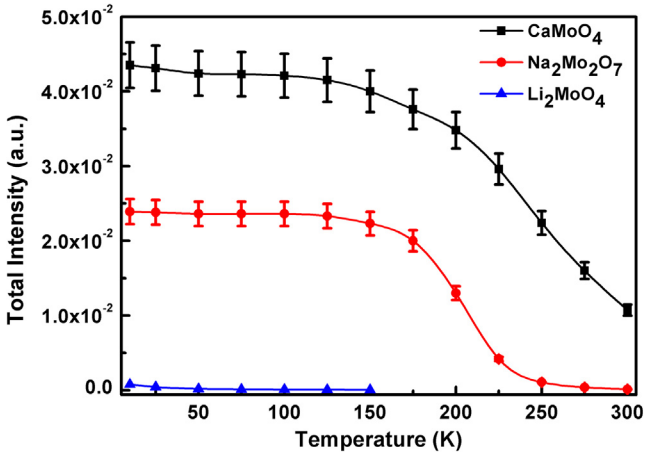

Fig. 6. Comparison of light yields of the $CaMoO_4$, $Na_2Mo_2O_7$, and Li_2MoO_4 crystals, at different temperatures, using a 280-nm-wavelength LED excitation source. The solid line in the figure is for guiding the eye.

300 K, which might result from the thermal quenching effect and the emission intensity decreases as the probability of non-radiative decays strongly increases with increasing the temperature [29]. The luminescence light yield increases with decreasing the temperature, and at 10 K the light yield of the $Na_2Mo_2O_7$ crystal is 55% that of the $CaMoO_4$ crystal. The light yield of the grown crystal could be increased in the future by using high-purity raw materials (Na_2CO_3, MoO_3), by improving the crystal growth conditions, and by optimizing the after-growth treatment.

Charge carrier trapping is one of the main issues associated with cryogenic scintillators, worsening the luminescence and scintillation properties at low temperatures [28]. In the reported molybdate crystals – Li_2MoO_4 (10 K to 50 K) [30], $SrMoO_4$ (32 K, 37 K, 50 K, 103 K, 112 K, 166 K, 205 K, and 238 K), $PbMoO_4$ (19 K, 43 K, 85 K, and 110 K), $CaMoO_4$ (20 K, 52 K, and 150 K), and $ZnMoO_4$ (35 K, 76 K, and 92 K) [28] – trap centers occurred, which reduced the luminescence intensity of these crystals. To study the trap centers in the $Na_2Mo_2O_7$ crystal, we performed TSL measurements, and the results are shown in Fig. 7. Clearly, there is one noticeable trap center that occurs at ~54 K and two low-intensity traps at 150 K and 210 K. The TSL peak intensities of the $Na_2Mo_2O_7$ and $CaMoO_4$ crystals were compared, and the peak intensity of the $Na_2Mo_2O_7$ crystal was found to be much weaker than that of the $CaMoO_4$ crystal. This result confirms a smaller light loss in the $Na_2Mo_2O_7$ crystal at low temperatures; thus, this crystal can be used as a cryogenic detector in future experiments.

Fig. 8 shows the luminescence spectra of the $CaMoO_4$, $Na_2Mo_2O_7$, and Li_2MoO_4 crystals, at 10 K. For the $Na_2Mo_2O_7$, $CaMoO_4$, and Li_2MoO_4 crystals, emission peaks are observed at 663 nm, 535 nm, and 526 nm, respectively. The peak intensity for the $Na_2Mo_2O_7$ crystal is weaker than that for the $CaMoO_4$ crystal; however, it is stronger than that for the Li_2MoO_4 crystal. From the emission

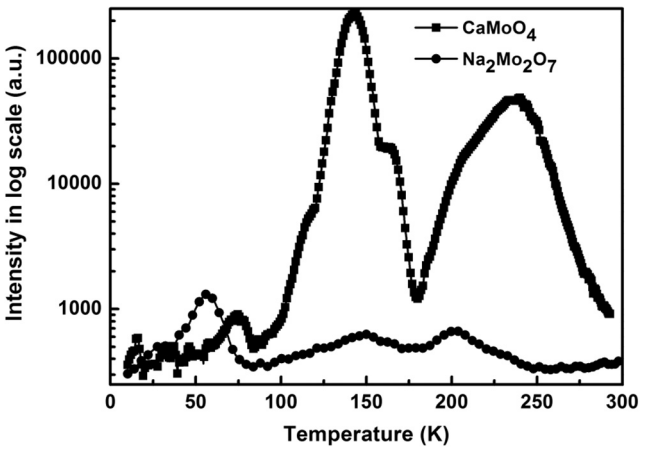

Fig. 7. Thermoluminescence glow curves of the $Na_2Mo_2O_7$ and $CaMoO_4$ crystals.

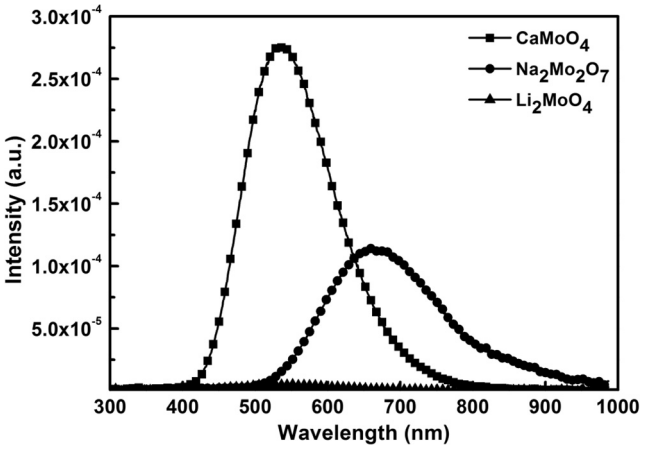

Fig. 8. Emission spectra of the $CaMoO_4$, $Na_2Mo_2O_7$, and Li_2MoO_4 crystals, at 10 K.

Table 1
Total luminescence intensities for the $CaMoO_4$, $Na_2Mo_2O_7$, and Li_2MoO_4 crystals, at 10 K.

Crystal	Total intensity (a.u.)
$CaMoO_4$	4.35×10^{-2} (100%) ±3.05×10^{-3}
$Na_2Mo_2O_7$	2.39×10^{-2} (55%) ±1.67×10^{-3}
Li_2MoO_4	7.95×10^{-4} (2%)

spectra at 10 K, we calculate the total intensity (light yield) of the Mo-containing crystals. The results, normalized to that of the $CaMoO_4$ crystal, are listed in Table 1. For each case, the total intensity (the area under the emission curve), was calculated from the corresponding emission spectrum using Eq. (2) [31]:

$$\text{Total intensity} = \sum \text{Em}(\lambda) * \Delta\lambda \quad (2)$$

where $\text{Em}(\lambda)$ is the emission probability at a given wavelength.

4. Conclusions

$Na_2Mo_2O_7$ single crystals having different (Ø20 × 35 mm^3 to Ø40 × 100 mm^3) size were grown for the first time using the Czochralski technique. The melting point of this scintillator was 603 °C, which is the lowest among the melting points of other reported Mo-containing crystals. XRD confirmed the orthorhombic crystal structure with the Cmca space group. The indirect energy band gap of the present crystal was found to be 3.05 eV. At 10 K, a broad-band emission in the 400–987 nm range, peaking at 663 nm, was observed, using 280-nm-wavelength UV light as the excitation source. However, the responses of scintillation materials to UV, alpha, beta, and gamma radiation may be different. Luminescence light yield enhancement was observed as the temperature decreased down to 10 K, and at this temperature the light yield was ~180 times higher than that at room temperature. Compared with $CaMoO_4$, at 10 K, the luminescence light yield of the grown crystal was 55%, even though it was much lower at room temperature. The light yield could be increased by improving the quality of the crystal and optimizing the after-growth heat treatment. The level of traps in the sample was measured for temperatures ranging from room temperature to 10 K, and the intensity of traps was found to be very low compared with that of the $CaMoO_4$ crystal. The hygroscopicity of the crystal was measured and found to be less than that of the Li_2MoO_4 crystal. Since $Na_2Mo_2O_7$ crystals are free of radioactive elements and exhibit high light yield at low temperatures, this material is a strong candidate for the search of neutrinoless double beta decay of ^{100}Mo and dark matter at cryogenic temperature.

Acknowledgments

This research has been supported by IBS-R016-D1-2014-a00 and the National Research Foundation of Korea (NRF) funded by the Korean government (MEST) (No2015R1A2A1A13001843).

References

[1] S.R. Elliott, Mod. Phys. Lett. A 27 (2012) 1230009 (16).
[2] Annika H.G. Peter et al., Phys. Dark Universe 5–6 (2014) 45.
[3] R. Steven, Elliott and Jonathan Engel, J. Phys. G: Nucl. Part. Phys. 30 (2004) R183–R215.
[4] M.C. Chen, J. Phys: Conf. Ser. 598 (2015) 012008.
[5] S. Rahaman et al., Phys. Lett. B 662 (2008) 111.
[6] H. Ejiri et al., Phys. Lett. B 258 (1991) 17.
[7] J. Meija et al., IUPAC Technical Report, Pure Appl. Chem. 88 (3) (2016) 293.
[8] F.A. Danevich et al., Nucl. Instrum. Meth. A 622 (2010) 608.
[9] Hua Jiang et al., J. Korean Phys. Soc. 63 (2013) 2018.
[10] V.B. Mikhailik et al., J. Phys.: Condens. Matter 20 (2008) 365219 (8pp).
[11] Ming-Xuan Xue et al., Chin. Phys. C 41 (2017) 046002.
[12] J.W. Beeman et al., Phys. Lett. B 710 (2012) 318.
[13] J.W. Beeman et al., Astropart. Phys. 35 (2012) 813.
[14] T.B. Bekker, et al, Astropart. Phys. 72 (2016) 38–45.
[15] S.J. Lee et al., Astropart. Phys. 34 (2011) 732.
[16] H. Bhang et al., J. Phys: Conf. Ser. 375 (2012) 042023 (4).
[17] V.B. Mikhailik, H. Kraus, Phys. Status Solidi B 247 (2010) 1583.
[18] V. Alenkov et al., JINST 8 (2013) P06002.
[19] K.W. Kim et al., Astropart. Phys. 62 (2015) 249.
[20] https://idm2016.shef.ac.uk/indico/event/0/session/11/contribution/144/material/slides/0.pdf
[21] R. Bernabei et al., Eur. Phys. J. C 73 (2013) 2648.
[22] R. Strauss et al., J. Phys.: Conf. Ser. 718 (2016) 042048.
[23] P. Meunier et al., Appl. Phys. Lett. 75 (1999) 1335.
[24] L. Berge et al., JINST 9 (2014) P06004.
[25] G.D. Saraiva et al., J. Raman Spectrosc. 42 (2011) 1114.
[26] Markus Meinert, Gunter Reiss, J. Phys.: Condens. Matter 26 (2014) 115503 (4pp).
[27] A.N. Annenkov et al., Nucl. Instrum. Meth. A 584 (2008) 334.
[28] D.A. Spassky et al., Opt. Mater. 35 (2013) 2465.
[29] V.B. Mikhailik et al., Phys. Rev. B 75 (2007) 184308 (6).
[30] D.A. Spassky et al., J. Lumin. 166 (2015) 195.
[31] Chunmeng Liu et al., Chem. Mater. 26 (2014) 3709–3715.